Electronic Supplementary Information

Block copolymer assisted synthesis of VO$_2$ (B) microflowers for supercapacitor application

Nitish Kumar,[a] Neetu Bansal,[a] Rahul R. Salunkhe[a,*]

Materials Research Laboratory, Department of Physics, IIT Jammu, Jammu and Kashmir (181221)

*Corresponding author: rahul.salunkhe@iitjammu.ac.in

Experimental details

Chemicals

Vanadium (V) oxide (V_2O_5, purity ≥98%), oxalic acid dihydrate (ACS reagent, purity≥99%), polyvinylpyrrolidone (PVP, M.W.= 10,000), and pluronic F-127 (M.W.=12,600) block copolymer were purchased from Sigma-Aldrich. All the chemicals were of analytic grade and were used directly without any further modification. Methanol (AR) and ultrapure water (18.2 MΩ) were used for washing samples.

Experimental synthesis of pristine VO_2 (B) [VP] and porous VO_2 (B) [VM]

For pristine VO_2 (B) synthesis, 1.27 mg of V_2O_5 was mixed in 70 ml of ultrapure water and stirred for 10 mins. The solution turns out to be yellow. Then, 1.765 mg of oxalic acid was added to the same. The solution color starts becoming light yellow indicating the reduction of V_2O_5. After stirring the solution for one hour, the solution was transferred to a 100 ml Teflon-lined autoclave. Further, the autoclave was put in a furnace to undergo hydrothermal reaction at 180 °C for 48 h by the heating rate of 5 °C·min^{-1}.

Porous VO_2 was also synthesized following the same steps. The difference, in this case, is that 1.764 g of F127 and 0.7 g of polyvinylpyrrolidone (PVP) were also added along with V_2O_5 and oxalic acid. After stirring for 1 h, this solution was also packed in an autoclave and was put for hydrothermal reaction under the same conditions. Both solutions (VP and VM) were let to cool down naturally at room temperature. Then solutions were filtered with a nylon filter paper (0.45 μm) using vacuum filtration assembly. The resultant blue-black precipitates were washed several times using ultrapure water and methanol. Then washed solutions were transferred to a petri dish and left to dry in the oven at 60 °C overnight. Both the samples were annealed at 350 °C for 3 h under the constant N_2 flow. This procedure helped in the removal of polymer templates from the material. The final product was washed with ultrapure water and dried in methanol.

Structural characterization

The structural properties of VO_2 were analyzed using powder X-ray diffraction (Panalytical Empyrean, Cu K-α, λ = 1.5406 Å). The PXRD experiments were performed at room temperature in reflection mode using Bragg Brentano incidence geometry and Galipix 3D detector. Morphology of VO_2 was characterized on field emission scanning electron microscope (FESEM) and transmission electron microscope (TEM). BET surface area measurement was done on Autosorb-iQ (Quantachrome) at 77 K. The chemical composition of the material was characterized using X-ray photoelectron spectroscopy, conducted at room temperature using a Nexsa (ThermoFisher Scientific) instrument with an Al Kα X-ray source.

Characterization for supercapacitor

All the electrochemical tests were done on an electrochemical workstation (CH instrument, CHI1150C). In the three-electrode configuration, synthesized VO_2 acted as working electrode, Ag/AgCl served as a reference electrode, and Pt wire was used as the counter electrode. We have utilized a 1 M Na_2SO_4 aqueous solution as the electrolyte. For the preparation of the working electrode, 80% wt of synthesized VO_2,10% wt.

of carbon black, and 10% wt. of polyvinylidene fluoride (PVDF) were mixed finely in a mortar pestle. This powder was further mixed with a few drops of 1-Methyl-2-pyrrolidine (NMP) to make a slurry. This slurry was drop-casted over graphite electrodes having an outer surface area of 1 cm^2. After drying, the electrode was used as a working electrode., The total mass loading over the graphite electrode was measured as 0.8 $mg.cm^{-2}$ using an ultra microbalance (Mettler Toledo).

We have used stainless steel (SS 304) disk electrodes of diameter 1.5 cm for two-electrode measurements. The total mass loading was 1 mg for both electrodes. We have used Whatman filter paper (pore size=0.45 μm) as the separator. Both the electrodes were packed inside the glove box in the HS flat cell (Hoshen corp.) arrangement. We have used organic electrolyte 2 M tetraethylammonium tetrafluoroborate (TEABF$_4$) in acetonitrile (ACN) for electrochemical device studies.

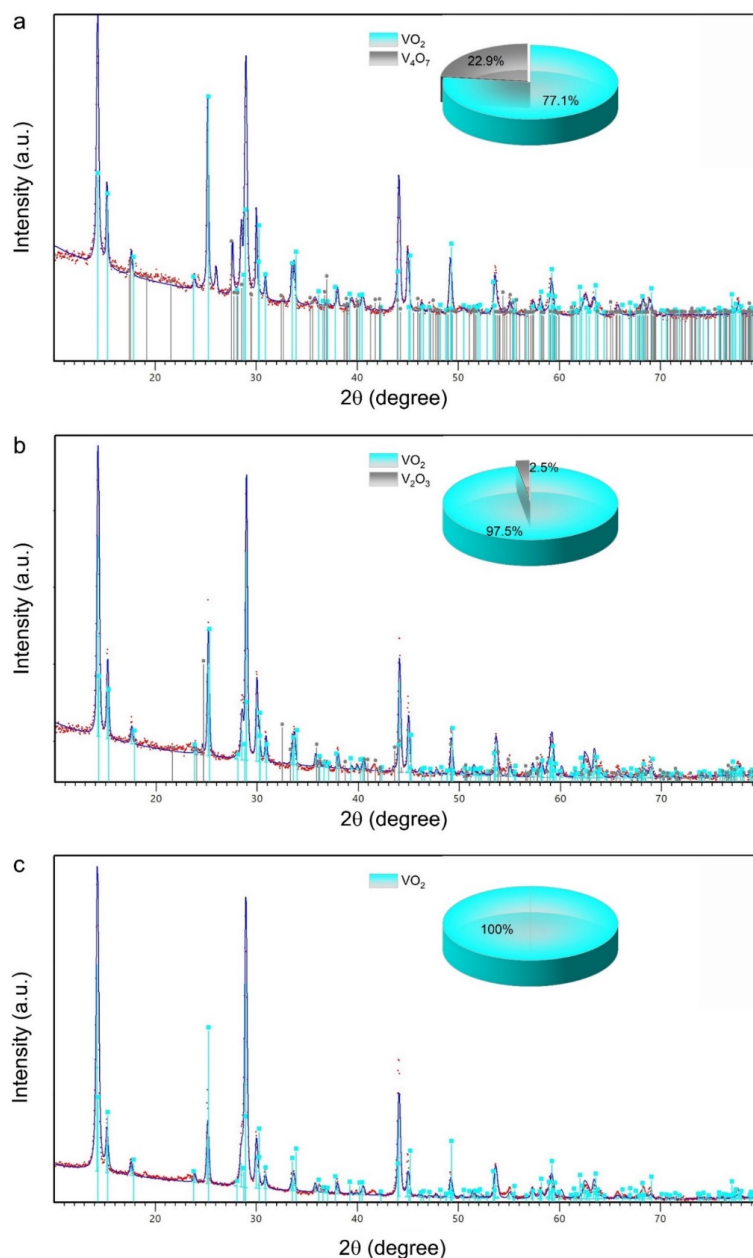The structure of the material has been optimized for the different reaction times of hydrothermal treatment.

Fig. S1. XRD analysis for optimizing the VO$_2$ phase. a) PXRD spectra for the sample synthesized by 24 h hydrothermal treatment. The Rietveld refinement shows the mixture of two oxidation states of vanadium. b) PXRD spectra for the sample synthesized by 36 h hydrothermal treatment, and c) PXRD spectra for the sample synthesized by 48 h hydrothermal treatment. The refinement spectra show the optimized single phase of VO$_2$. All Rietveld refined studies were performed using High Score Plus software.[1]
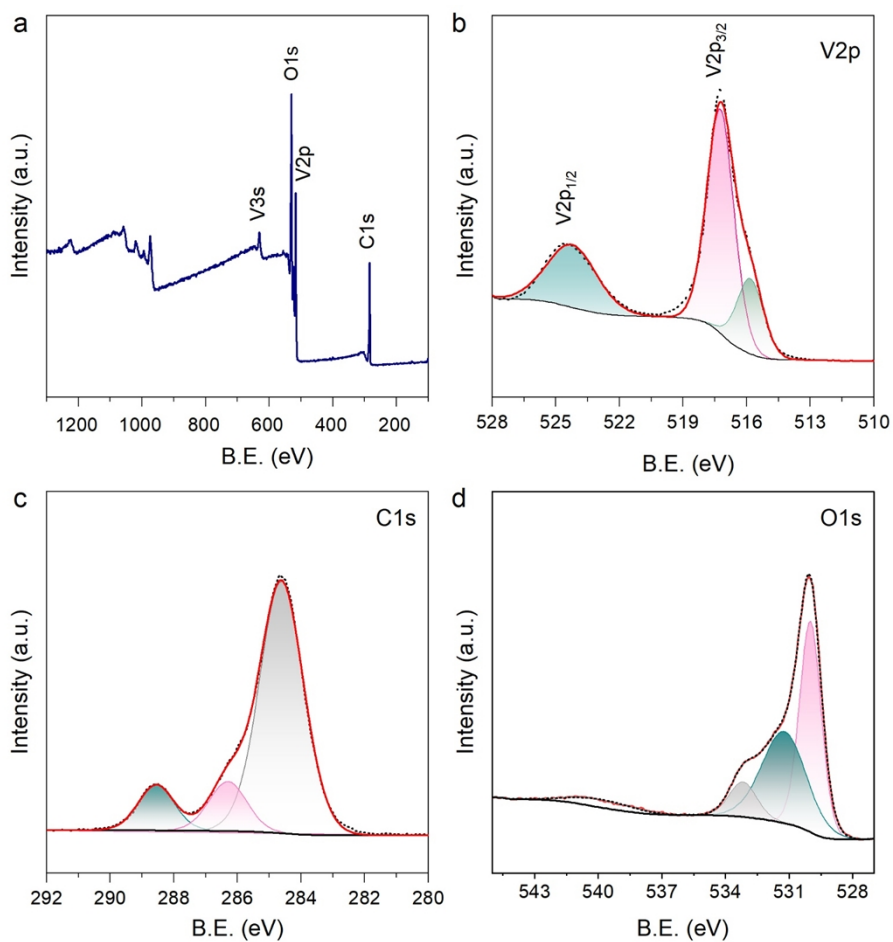
Fig. S2. XPS study for VP sample. a) Survey spectra show vanadium, oxygen, and carbon in the sample. Narrow region spectra for b) V 2p, c) C 1s, and d) O 1s.
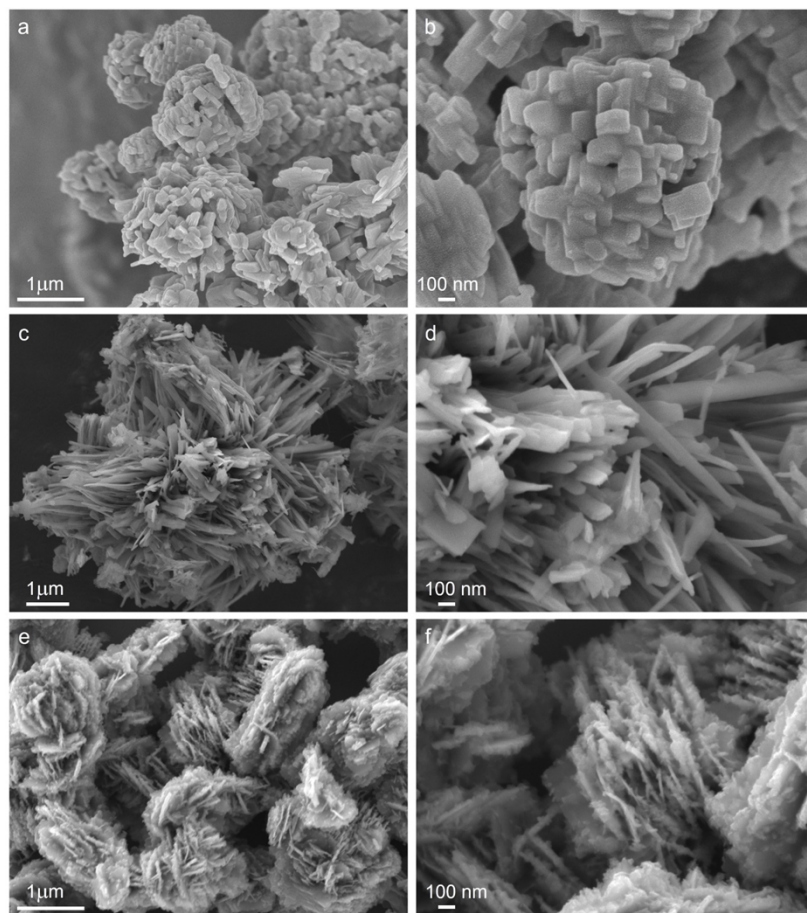
Fig. S3. Morphological optimizations. FESEM images of different VO$_2$ samples at different magnifications. (a-b) pristine VO$_2$, (c-d) only F127 addition, and (e-f) solely PVP addition.
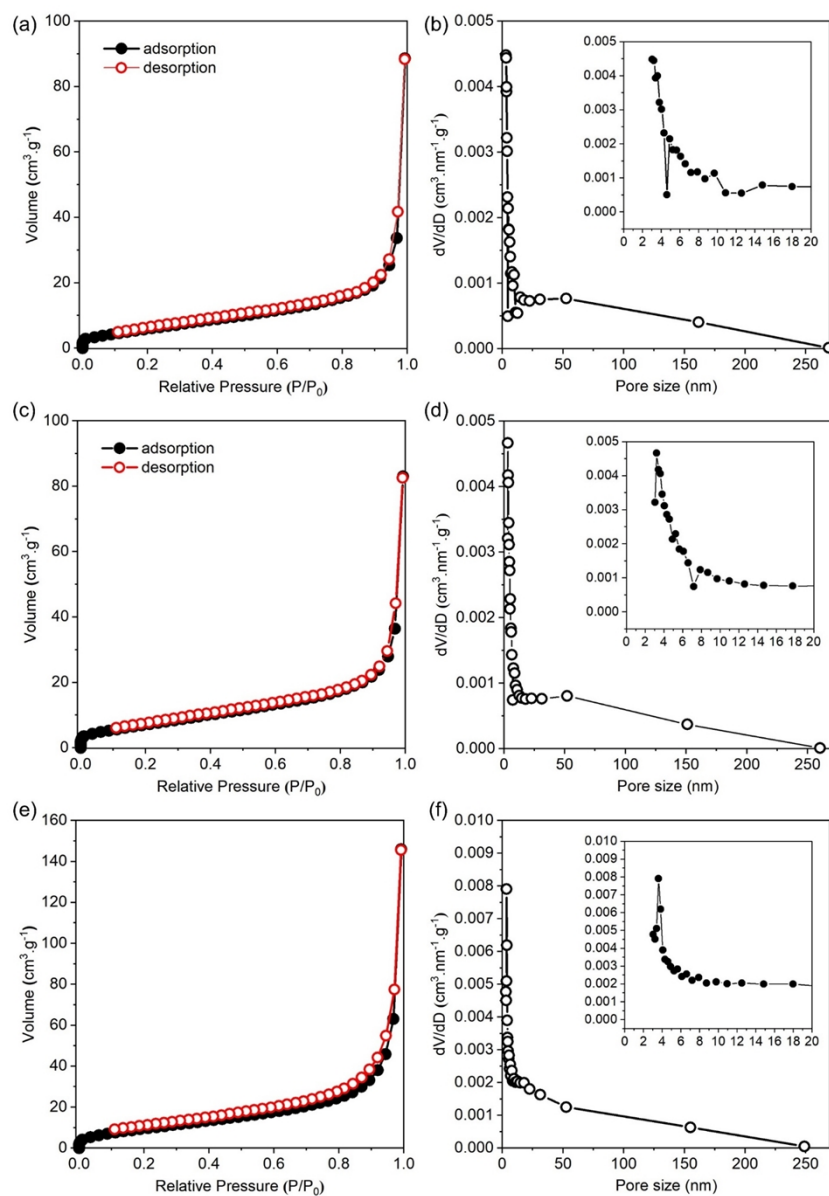
Fig. S4. Surface area and pore size comparison for various VO$_2$ samples. Adsorption-desorption isotherms at 77 K for N$_2$ gas adsorption for a) pure VO$_2$, c) VO$_2$ modified solely by PVP, and e) VO$_2$ modified solely by F127. Pore size distribution using BJH model on desorption curve for b) pristine VO$_2$, d) VO$_2$-PVP, and f) VO$_2$-F127.
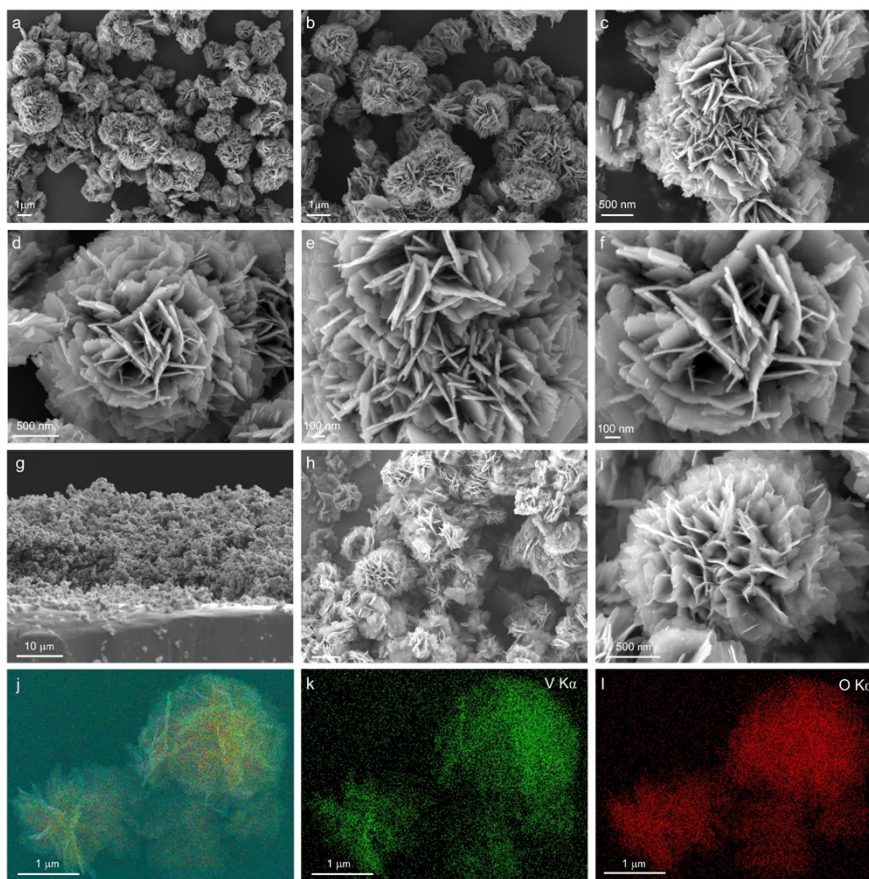
Fig. S5. FESEM images of optimized VM samples at different magnifications. a, b) Lower magnification FESEM showing the uniform morphology of the sample. c, f) High magnification images showing the nanosheets assembled in microflower shape, the individual sheet without having any agglomeration can be observed clearly. g-i) cross-sectional FESEM images at various magnifications, further supporting the homogeneous and uniform sample claim. j-l) EDS images showing the presence of V and O in the sample.

Table S1. Three electrode supercapacitor performance comparison.

Material	Specific capacitance $(F.g^{-1})$	Current density $(A.g^{-1})$	Voltage window (V)	Electrolyte	Mass loaded $(mg.cm^{-2})$	References
Hydrogen treated VO_2	300	1	0.8	1M Na_2SO_4	-	[2]
$VO_2(A)$@carbon	179	1	0.8	0.5M Na_2SO_4	4	[3]
$VO_2(A)$	70					
$VO_2(B)$/CNTs	250	0.5	1.8	1M Na_2SO_4	-	[4]
$VO_2(B)$	174					
$VO_2(B)$/rGO	353	1	1	0.5M K_2SO_4	0.025mg	[5]
$VO_2(B)$	248					
2D VO_2 microarrays	275	0.5	0.6	1M Na_2SO_4	-	[6]
$VO_2(B)$/graphene	197	0.5	0.6	0.5M Na_2SO_4	3-5 mg	[7]
$VO_2(B)$	99					
VO_2@CC	180.3	0.5	1.65	15M LiTFSI	1.6	[8]
VO_2	191	1	1.2	0.5M K_2SO_4	1mg	[9]
VO_2	136	0.25	1.2	0.5M K_2SO_4	3mg	[10]
VO_2 hollow spheres	336	2 $mA.cm^{-2}$	1.5	1M Na_2SO_4/CMC	3.5	[11]
VM sample	395	5 $mV.s^{-1}$	0.8	1M Na_2SO_4	0.5	This Work

* *Carbon nanotubes (CNT), reduced graphene oxide (rGO), carbon cloth (CC)*

Table S2. Morphology and corresponding surface area comparison with recent literature reports.

Material	Method	Morphology	Surface Area $(m^2 \cdot g^{-1})$	References
Hydrogen treated VO$_2$	Reduced in a hydrogen atmosphere	-	8.64	[2]
2D VO$_2$ microarrays	Liquid interface derived method	Needle-like arrays	80	[6]
3D VO$_2$ (B)	Hydrothermal	Hollow spheres	29	[11]
VO$_2$ nanoplate	Hydrothermal	Coin shaped nanoplates	23.8	[12]
VO$_2$	Solvothermal	Yolk-shell	26.67	[13]
VO$_2$ (M)	Hydrothermal	Nanobelts	29	[14]
VO$_2$ (A)	Solvothermal	Nanorods	34.14	[15]
VO$_2$ (B)	Solvothermal	Nanosheets	23.82	[15]
VM sample	Hydrothermal	Microflowers	66.3	This Work

Table S3. Specific capacitance with surface area comparison for various vanadium oxides.

Material	Specific capacitance $(F.g^{-1})$	Current density $(A.g^{-1})$	Surface area $(m^2.g^{-1})$	References
Hydrogen treated VO_2	300	1	8.64	2
2D VO_2 microarrays	275	0.5	80	6
VO_2 hollow spheres	336	-	29	11
V_2O_5 nanowires	65	0.25	35.1	16
V_2O_3 bulk	159	0.05	8	17
Flowerlike V_2O_3	218	0.05	13.5	18
V_2O_5 nanowires	200	0.1	123	19
V_4O_9 microflowers	392	0.5	107.9	20
VO_2 microflowers (VM)	395	$5\ mV.s^{-1}$	66.3	This Work

Note S1. Extended electrochemical studies

GCD data for both VP and VM are compared at 0.1 A.g^{-1} and 0.5 A.g^{-1} current densities, as shown in Fig. S6 (c). The VP shows less charging/discharging time in comparison to VM. The VM takes advantage of its porous structure and improved conductivity and consequently exhibits improved performance.

Further, the EIS data was studied extensively for both samples. The experimental data were compared with the simulated data based on the Randles circuit, as shown in the inset of Fig. 3 (d). The comparative Nyquist plot at the frequencies from 100 kHz to 100 mHz is shown in Fig. 3 (d), while for frequencies 100 kHz to 10 mHz is shown in Fig. S6 (d). The intercept in the x-axis shows the total internal resistance (R_S), whereas the diameter of the semi-circular region is indicated as charge transfer resistance (R_{CT}). The equivalent circuit resembles the Randles circuit, which yields the R_S and the parallel connection of R_{CT} and $C_{DL,}$ representing the small arc in the high-frequency section where C_{DL} originates from double-layer capacitance.[21] The constant phase element (CPE) represents the double layer capacitance occurring at the interface between the electroactive material and the electrolyte. The Warburg element (W) represents the impedance due to the diffusion of electrolyte ions within pores of the VO$_2$ electrode is represented by the Warburg element (W). It is dependent upon the frequency, whereas R_L represents the leakage resistance during the electrochemical activities.[22] The pristine VO$_2$ exhibits R$_s$ and R$_{CT}$ values of 7.2 and 87 Ω, respectively, while the porous VO$_2$ have R$_s$ and R$_{CT}$ values as 5.5 and 17 Ω correspondingly. The main reason behind this improved conductivity is the porous structure and the reduced agglomeration at the electrode-electrolyte interface.

Moreover, the cyclic stability results for the VM sample further support its good stability as it exhibits 72% of capacitance retention even after 5000 charge-discharge cycles. The capacitance reduction with the increasing number of charge-discharge cycles is common for metal oxides because of the constant redox reactions during charging and discharging cycles. Consequently, the metal oxide lattice becomes strained, and the performance is affected.[21] The slightly increased performance after 2500 cycles is the material activation by the diffusion of electrolyte ions inside the pore channels in the VO$_2$ microflowers. As this process is lengthy and complex at the atomic level, some environmental factors can play a role during a long experimental time; hence, we have introduced the error bars (~ 3%) in the cyclic stability plot to show practical errors during this measurement.
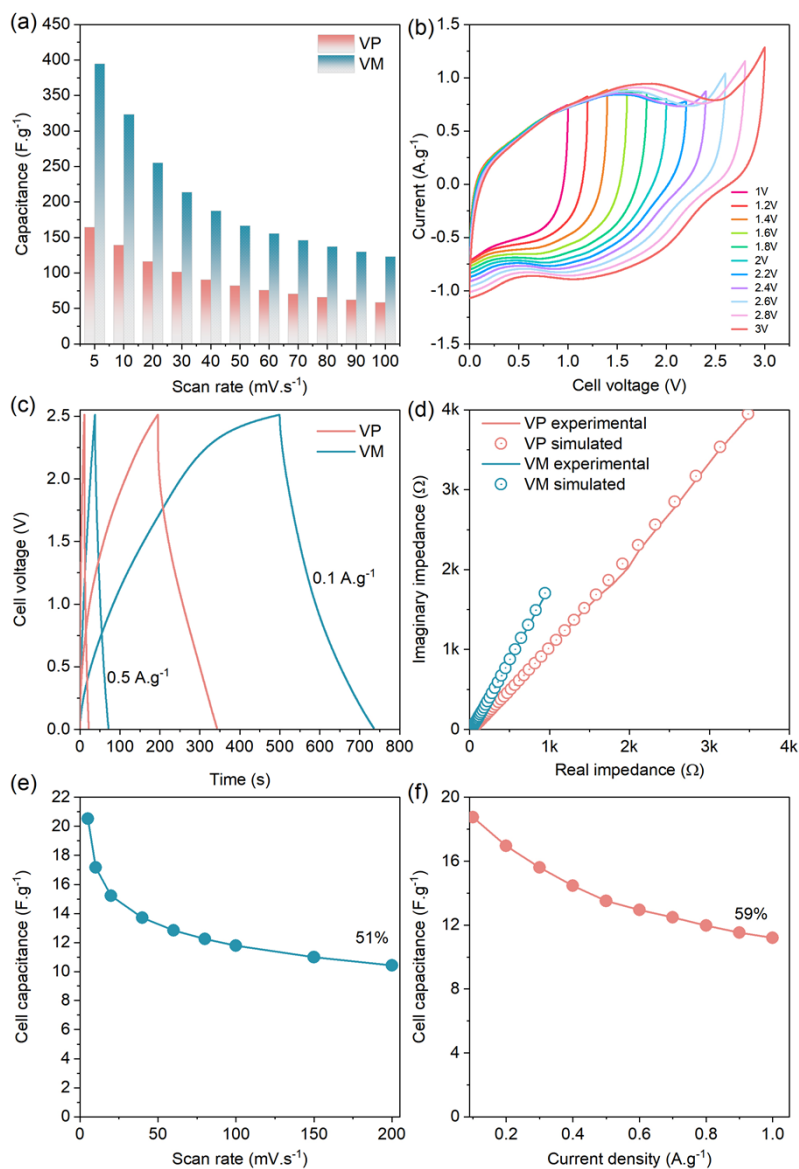
Fig. S6. Detailed SC study for porous vanadium oxide. a) Comparative capacitance retention with scan rate variation shown by bar graph for VP and VM. b) Voltage window extension curves for assembled symmetric supercapacitor device using VM as electrodes. c) Comparative charge-discharge curves for VP and VM samples. d) Comparative Nyquist plots for both samples and e) cell capacitance vs. scan speed for CV measurements of device. f) Cell capacitance vs. current density, showing that capacitance retains about 60% even at ten times higher scan rates.
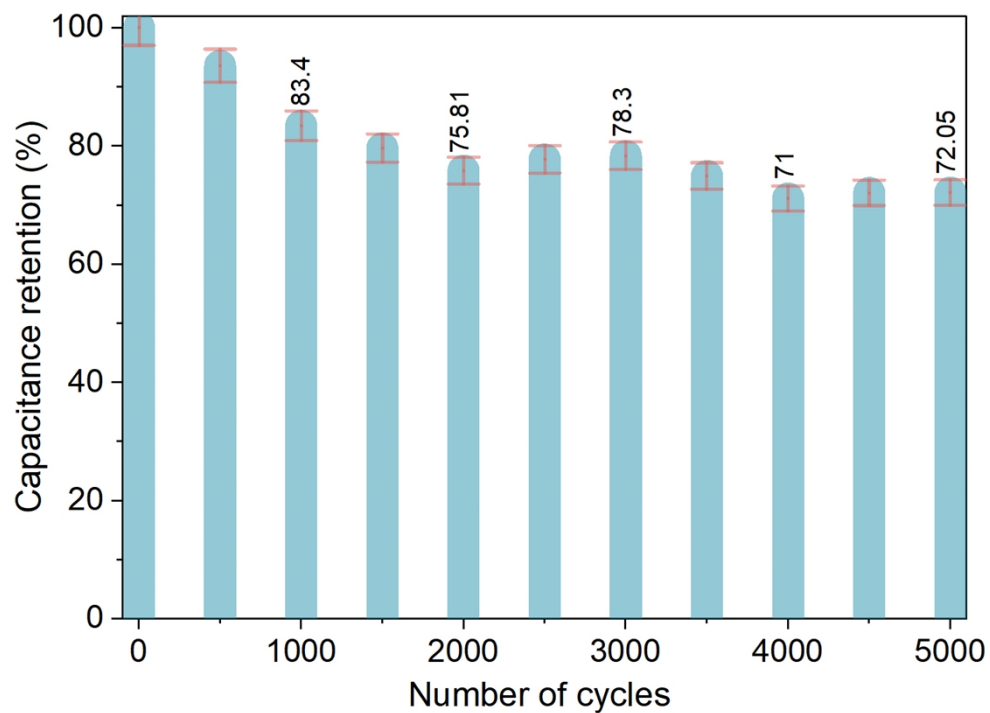
Fig. S7. Cyclic stability test for symmetric supercapacitor device for VM sample. The error bars (~ 3%) account for variation in environmental conditions during long experimental times.

Table S4. Data summary.

Rietveld refined lattice parameters					
a(Å)	b(Å)	c(Å)	α(º)	β(º)	γ(º)
12.049	3.695	6.435	90	107.05	90

XPS data		
Element	B.E. (eV)	Atomic %
V	516.1	20.80
O	530.1	35.89
C	284.7	43.31

BET data			
Sample	Surface area ($m^2.g^{-1}$)	Pore volume ($cc.g^{-1}$)	Average pore diameter (nm)
VP	28.7	0.122	17.8
VM	66.3	0.247	14.9

SC data		
Sample	Specific capacitance ($F.g^{-1}$)	Scan rate ($mV.s^{-1}$)
VP	160	5
VM	395	5
	323.3	10
	254.9	20
	213.7	30
	187.4	40
	166.6	50
	155.7	60
	146.2	70
	136.8	80
	129.7	90
	123.2	100

EIS data		
Sample	R_s (Ω)	R_{ct} (Ω)
VP	7.2	87
VM	5.5	17

References

1   T. Degen, M. Sadki, E. Bron, U. König and G. Nénert, *Powder Diffr.*, 2014, **29**, S13–S18.

2   X. Pan, Y. Zhao, G. Ren and Z. Fan, *Chem. Commun.*, 2013, **49**, 3943.

3   J. Zheng, Y. Zhang, Q. Wang, H. Jiang, Y. Liu, T. Lv and C. Meng, *Dalt. Trans.*, 2018, **47**, 452–464.

4   L. Liang, H. Liu and W. Yang, *J. Alloys Compd.*, 2013, **559**, 167–173.

5   W. Lv, C. Yang, G. Meng, R. Zhao, A. Han, R. Wang and J. Liu, *Sci. Rep.*, 2019, **9**, 10831.

6   Y. Fan, D. Ouyang, BW. Li, F. Dang and Z. Ren, *Nanoscale Res. Lett.*, 2018, **13**, 142.

7   J. Zhang, L. Chen, Y. Wang, S. Cai, H. Yang, H. Yu, F. Ding, C. Huang and X. Liu, *Nanomaterials*, 2018, **8**, 1020.

8   S. Chen, H. Yu, L. Chen, H. Jiang and C. Li, *Chem. Eng. J.*, 2021, **423**, 130208.

9   H. Wang, H. Yi, X. Chen and X. Wang, *J. Mater. Chem. A*, 2014, **2**, 1165–1173.

10   L. Deng, G. Zhang, L. Kang, Z. Lei, C. Liu and Z.-H. Liu, *Electrochim. Acta*, 2013, **112**, 448–457.

11   Y. Zhang, X. Jing, Y. Cheng, T. Hu and M. Changgong, *Inorg. Chem. Front.*, 2018, **5**, 2798–2810.

12   Z. Cao, L. Wang, H. Zhang, X. Zhang, J. Liao, J. Dong, J. Shi, P. Zhuang, Y. Cao, M. Ye, J. Shen and P. M. Ajayan, *Adv. Funct. Mater.*, 2020, **30**, 2000472.

13   Z. Song, X. Lu, Q. Hu, D. Lin and Q. Zheng, *Dalt. Trans.*, 2020, **49**, 14921–14930.

14   M. Aziznezhad, E. Goharshadi and M. Namayandeh-Jorabchi, *Sol. Energy Mater. Sol. Cells*, 2020, **211**, 110515.

15   N. M. Ndiaye, T. M. Masikhwa, B. D. Ngom, M. J. Madito, K. O. Oyedotun, J. K. Dangbegnon and N. Manyala, *Mater. Chem. Phys.*, 2018, **214**, 192–200.

16   L. Deng, Y. Gao, Z. Ma and G. Fan, *J. Colloid Interface Sci.*, 2017, **505**, 556–565.

17   H. Y. Li, K. Jiao, L. Wang, C. Wei, X. Li and B. Xie, *J. Mater. Chem. A*, 2014, **2**, 18806–18815.

18   H. Liu, Y. Wang, H. Li, W. Yang and H. Zhou, *ChemPhysChem*, 2010, **11**, 3273–3280.

19   A. Qian, K. Zhuo, M. S. Shin, W. W. Chun, B. N. Choi and C.-H. Chung, *ChemSusChem*, 2015, **8**, 2399–2406.

20   H. Pang, Y. Dong, S. L. Ting, J. Lu, C. M. Li, D. H. Kim and P. Chen, *Nanoscale*, 2013, **5**, 7790.

21   L. Li, Z. A. Hu, N. An, Y. Y. Yang, Z. M. Li and H. Y. Wu, *J. Phys. Chem. C*, 2014, **118**, 22865–22872.

22   R. Sahoo, T. H. Lee, D. T. Pham, T. H. T. Luu and Y. H. Lee, *ACS Nano*, 2019, **13**, 10776–10786.